

Short Communication

## Development Zinc Oxide–Cotton Fibers as Anode Materials for Lithium-Ion Batteries

Hongqiang Wan<sup>\*</sup>, Peiying Han, Shuai Ge, Fancong Li, Simiao Zhang and Huan Li

Mechanical and Electrical Engineering Institute, Xi'an Technological University, Shaanxi, Xi'an, 710600, China

\*E-mail: [hqwmql@sina.cn](mailto:hqwmql@sina.cn)

Received: 2 January 2018 / Accepted: 24 February 2018 / Published: 10 April 2018

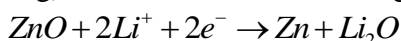
The deposition of synthesized zinc oxide nanoparticles on the surface of cotton fiber under ultrasonic irradiation was reported in this study. The presence of the hexagonal phase of the crystalline metal oxide was confirmed by the XRD results. We also studied the electrochemical features of ZnO employed as an anode material for lithium-ion batteries. ZnO showed favorable lithium storage properties.

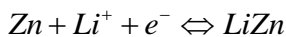
**Keywords:** Energy storage; Electrochemical performance; Cotton; Li-ion battery; Zinc oxide

### 1. INTRODUCTION

Zinc oxide (ZnO) is considered one of the most promising semiconductor materials in the photonics and electronics fields due to its wide band gap and large exciton binding energy (3.4 eV and 60 meV, respectively) [1, 2]. Therefore, tremendous attention has been paid to the synthesis and use of the nano-metal oxide coatings on cotton and glass substrates [3-6]. To avoid potential nosocomial infections, antibacterial fabrics, such as medical clothes, protective garments, and bed spreads, have attracted increasingly more attention [7-9]. Nanoparticles have distinct chemical and physical properties as well as high surface areas, and therefore, they have been recognized as more active than larger ones [10-15].

ZnO is abundant, non-hazardous, and low cost and has been accepted as an active material for Li-ion battery anodes [16-18]. ZnO shows Li-storage/extraction reactions (total theoretical capacity, 960 mAh/g), as shown in the following reactions:





For bulk ZnO, Zn, and Li<sub>2</sub>O, the molar volumes are 14.6, 18.3, and 14.6 cm<sup>3</sup>/M, respectively. The results imply a consistent volumetric change of 231 % from ZnO to Zn and Li<sub>2</sub>O during Li insertion in equation (1). Pulverization and electrical isolation in the active material are caused by large-scale volume expansion; accordingly, the capacity and cycling performance decrease. In addition, the faded performance also results from the low electronic conductivity and the slow kinetics of Li-ion diffusion in Zn and ZnO [19-22]. The performance improvement has been studied using the size reduction of ZnO. Unfortunately, a significant improvement has not been realized for nanosized ZnO electrodes [23-25]. Therefore, GD-film electrodes were proposed in this report and were fabricated based on a one-step precipitation technique with prepared microstructured ZnO. Several research groups, such as Yamabi and co-workers [26], Vayssieres and co-workers [27], and Li and co-workers [28], proposed the above preparation route as a large-scale approach. One-dimensional crystalline ZnO can be produced using this route under mild conditions, atmospheric pressure and moderate temperatures (< 90 °C) in a strongly basic aqueous solution containing Zn(OH)<sub>4</sub><sup>2-</sup> [29-33]. Based on the previous literature, the morphological control of ZnO was studied, suggesting easy control of the ZnO microstructure through the addition of surfactants into solution or alteration of the growth conditions [34-39].

The present work reported the synthesis of ZnO nanoparticle-modified cotton fibers, along with the investigation of their electrochemical Li-insertion/extraction characteristics. In addition, the behavior of the composite electrodes was studied, as were the effects of the structure on their cycling performance.

## 2. EXPERIMENTS

Zinc sulfate, ethanol, and sodium hydroxide were commercially available from MERCK and used without further purification. Cotton was commercially available from a local market.

First, cotton fibers were washed in a water bath containing 5 % sodium dodecyl sulfate (SDS) for 60 min at 40 °C. Then, they were rinsed using distilled water and left drying under vacuum for 1 d at 60 °C. For the preparation of the ZnO-decorated cotton material, we first soaked the dry cotton (0.05 g) in 10 ml of distilled water containing 0.12 g of a ZnSO<sub>4</sub>·5H<sub>2</sub>O solution in a sonicated flask under irradiation for 10 min or 1 h using an ultrasonic generator Model US-150 Ti-horn (20 kHz, output 10 turning 7) (ZnO-10 and ZnO-60). The as-prepared mixture was further mixed with 0.06 g NaOH and stirred, followed by sonication again for 60 min over a temperature range of 35–40 °C. In addition, the bath temperature was kept constant at ~ 40 °C. For the removal of excess hydroxide, the resulting product was completely washed several times using distilled water and then left to dry under vacuum overnight at a temperature of 60 °C. In addition, the concentration of zinc in the fiber was measured using a titration method (3–4 wt%).

The electrochemical experiments were carried out using coin cells (CR2430) at 25 °C, where a pure lithium foil served as the reference and counter electrode. Furthermore, the working electrode was the ZnO sample obtained on zinc foil. The needle-like ZnO electrodes and bramble-like ZnO

electrodes exhibited mass loadings of 1.0 mg/cm and 1.2 mg/cm<sup>2</sup>, respectively. The fabrication of the cells was performed in a glove box under a dew point < -65 °C under an argon atmosphere. Additionally, the test electrolyte was prepared by dissolving 1 M LiPF<sub>6</sub> in a mixed solution of ethylene carbonate, dimethyl carbonate, and diethyl carbonate (volume ratio, 1:1:1) with a microporous polypropylene film as the separator. The galvanostatic charge/discharge measurements were conducted using the test cells. The charge/discharge experiments were conducted using a LAND battery program-control test system (CT 2001A, Wuhan Jinnuo Electronic Co., Ltd. of China) in a cut-off potential window of 0.005 to 2.4 V (constant current rate, 100 mA/g). Cyclic voltammetry (CV) experiments were performed using a CHI660D electrochemical workstation (scan rate, 0.1 mV/s; potential range, 0–3.0 V). The morphology was characterized via a Hitachi S3400N scanning electron microscope (SEM).

### 3. RESULTS AND DISCUSSION

For the preparation of the ZnO-modified fibers, we deposited ZnO nanoparticles onto cotton fibers using ultrasonic irradiation of a metal hydroxide, as shown in the following reactions:



The fresh product, Zn(OH)<sub>2</sub>, immediately dissolved, and superfluous Zn(OH)<sub>4</sub><sup>2-</sup> and OH<sup>-</sup> were generated. When the reaction solution pH reaches a certain value, the Zn(OH)<sub>4</sub><sup>2-</sup> generated herein would be converted to ZnO nanoparticles, as shown in the phase stability diagram of ZnO [40].

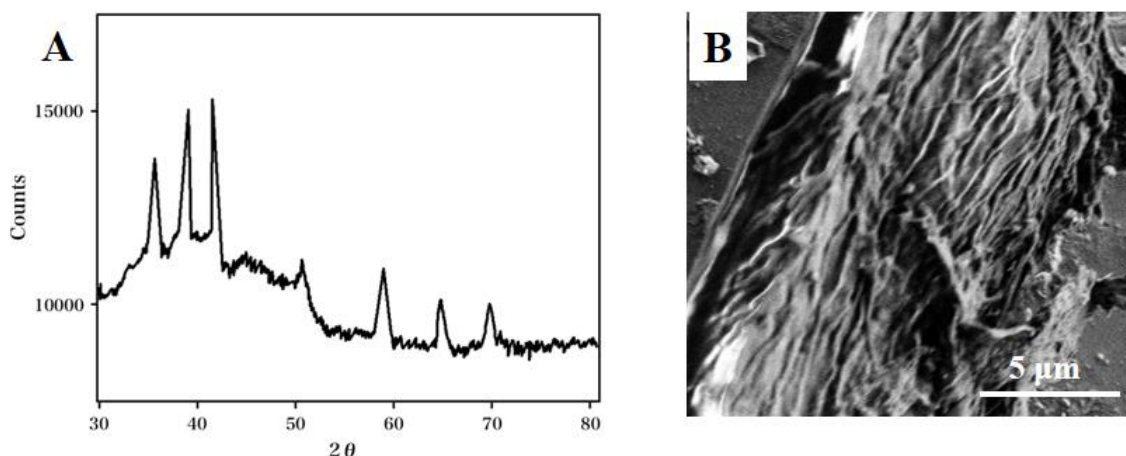


**Figure 1.** (A) XRD pattern and (B) SEM image of ZnO-modified cotton fibers.

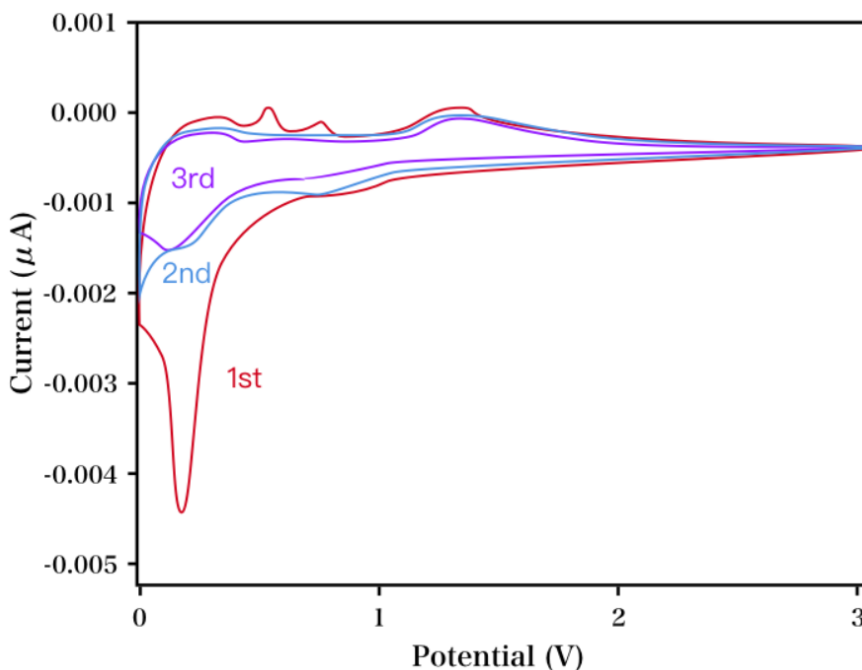
Through the sonochemical microjets formed by the collapse of sonochemical bubbles, the ZnO nanoparticles formed during the reaction may be physically adsorbed onto the cotton fiber surface [41]. The above nanoparticles remained on the surface after washing several times, showing strong physical adsorption on the cotton substrate. However, several ZnO nanoparticles with weak adsorption on the

fibers leached out during the initial five wash cycles, which necessitates washing the modified cotton composites prior to the drying treatment. Meanwhile, between pH 3 and 6, they show high stability; when the pH is lower than 3, they exhibit lower stability in which the acidic solution reacts with most of the ZnO particles.

The crystalline metal oxide was present on the cotton fibers, as shown in the X-ray diffraction (XRD) spectrum in Figure 1A. This profile is consistent with the hexagonal phase of ZnO [42], while very broad peaks appeared due to the nanosized crystallites. Additionally, this profile corresponds to the (1 0 0), (0 0 2), (1 0 1), (1 0 2), (1 1 0), (1 0 3) and (1 1 2) planes of wurtzite crystals. UV-vis and FTIR spectroscopies were also carried out to study the structural properties of the nanoparticles. An absorption band was observed at 359 nm for the ethanolic solution of the ZnO nanoparticles, as shown in the UV-vis spectrum. An absorption band was observed at  $466\text{ cm}^{-1}$  after immobilization of the ZnO nanoparticles on the cotton, which resulted from the lattice vibrations of the Zn-O bond. Additionally, the asymmetric stretching vibration of the bridging Zn-O-Zn gave rise to a strong band located at  $1,092\text{ cm}^{-1}$ . A broad band was observed at  $3,437\text{ cm}^{-1}$ , corresponding to O-H stretching; the absorption band located at  $1,553\text{ cm}^{-1}$  was assigned to the bending of the hydroxyl groups of some Zn(OH)<sub>2</sub> and/or physically adsorbed water molecules [43]. The morphology of the ZnO-modified cotton fibers is shown in Figure 1B.

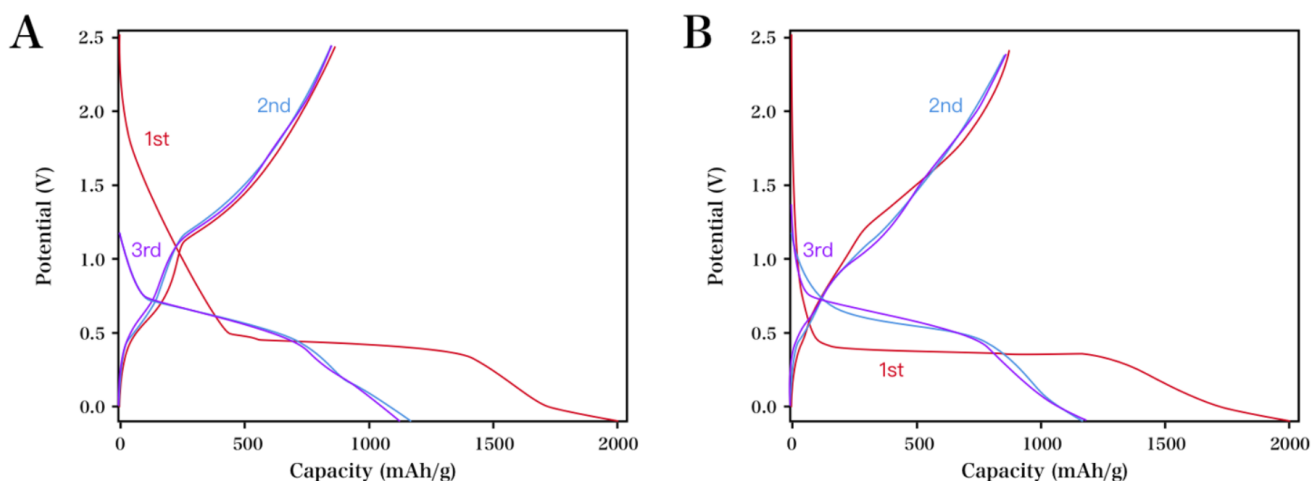
The electrochemical reactions of the ZnO electrodes were studied by performing a series of CV experiments over a potential range of 0 to 3 V vs. Li/Li<sup>+</sup>. We selected the first three cycles of the CVs recorded for the ZnO-10 electrode due to the similarity between the CVs of the two electrodes, (Figure 2). In the initial cathodic scan, one single significant peak was seen at approximately 0.2 V, which resulted from the reduction of ZnO into Zn, the generation of Li<sub>2</sub>O and a Li-Zn alloy, and the growth of a solid electrolyte interphase (SEI) layer [44]. As an organic film, the SEI layer was composed of LiF, ethylene oxide-based oligomers, lithium alkyl carbonate, and Li<sub>2</sub>CO<sub>3</sub> [45]. We only observed a single significant peak due to the similarity of the reaction potentials for of these reactions. A few insignificant peaks were recorded in the range of 0.5 to 0.8 V (resulting from the multi-step dealloying process of the Li-Zn alloy), along with a broad peak located at 1.4 V (associated with the decomposition of Li<sub>2</sub>O) during the initial anodic scan [46]. During the following two cycles, the cathodic peak located at 0.2 V was replaced by another peak at 0.6 V, which was possibly due to severe lithium intercalation and activation of the electrode [47]. During the two cycles, the position of the anodic peak was almost the same as that of the initial cycle (approximately 1.4 V). In addition, it is worth noting that the CV patterns recorded for cycles 2 and 3 almost overlapped, which suggests that the electrochemical reactions began to stabilize.

For these two ZnO samples, the galvanostatic discharge/charge curves during the first three cycles are shown in Figure 3 (current density, 100 mA/g). For the initial discharge cycle, the two electrodes showed a long potential slope over the range of 0.4 - 0.5 V, implying that the generation of an SEI layer may cause the initial irreversible capacity loss. For the discharge curves during the initial cycle, the slopes shifted to approximately 0.7 V; both electrodes showed similar curve shapes for the subsequent cycles. These results imply the reversibility of the lithiation process in ZnO.



**Figure 2.** The first three CV patterns recorded for the ZnO-10 electrode; scan rate: 0.1 mV/s.

During the first three cycles, both electrodes exhibited similar charge curve shapes, with the same potential slopes shown at 0.6 V (associated with the multi-step delithiation process of the lithium–zinc alloy) and 1.4 V (due to the formation of ZnO). ZnO-10 exhibited a significantly higher initial discharge/charge capacity (2,051 and 1,044 mAh/g, respectively) than the ZnO-60 electrode. In addition, the ZnO-60 and ZnO-10 electrodes each showed a low initial columbic efficiency of 42 and 54 %, respectively. The main reason for the low values is the irreversible capacity, which arises after the electrolyte decomposes and the SEI film forms. Additionally, the irreversible capacity cannot be avoided for most anodes. Table 1 summarizes some recent studies of anode materials for lithium-ion batteries. The specific capacity of our Fe<sub>2</sub>O<sub>3</sub>/TiO<sub>2</sub> anode was higher than those reported values for others at similar current densities. In addition, our ZnO-10 hybrid also exhibited good cycling stability.

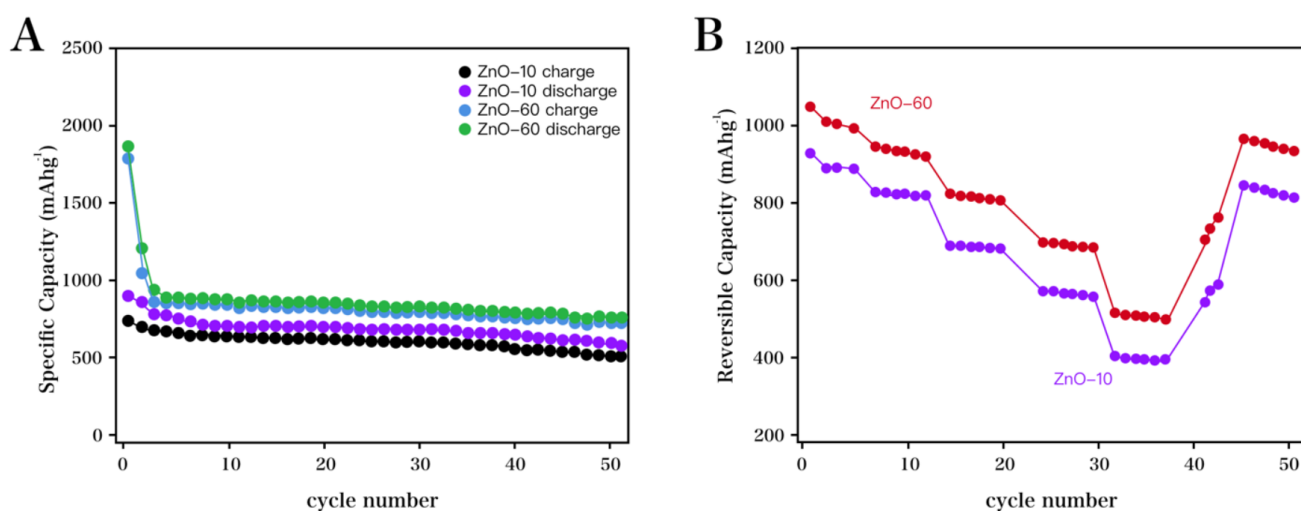


**Figure 3.** Galvanostatic discharge/charge patterns recorded for ZnO-10 and ZnO-60.

**Table 1.** List of recent studies of anode material for lithium-ion batteries.

Material	Current rate (mA/g)	Cycle numbers	Reversible capacity (mA/hg)	Reference
TiO <sub>2</sub> -B@Fe <sub>2</sub> O <sub>3</sub>	100	50	709	[48]
Co <sub>3</sub> O <sub>4</sub> /TiO <sub>2</sub>	100	120	660	[49]
TiO <sub>2</sub> @Fe <sub>2</sub> O <sub>3</sub>	100	100	520	[50]
TiO <sub>2</sub> @MnO <sub>2</sub>	355	100	350	[51]
TiO <sub>2</sub> @Fe <sub>2</sub> O <sub>3</sub>	100	100	617	[52]
ZnO-cotton fiber	100	50	777	This work

The cycle performances of both electrodes were studied in this work. The initial reversible capacity of the ZnO-10 electrodes was high, followed by a gradual decrease to 600 mAh/g after 50 cycles for the cell (capacity retention, 64 %). The cycling stability and reversible capacity of the ZnO-60 electrode were more favorable than those of the ZnO-10 electrode. The capacity remained at 777 mAh/g after 50 cycles (retention capacity rate, 73 %). However, the rate capability of ZnO-60 was also more desirable than that of the ZnO-10, as shown in the comparative analysis in Fig. 4B. After 10 cycles at 100 mA/g, both electrodes showed a stepwise increase in the current density up to 800 mA/g (Fig. 4B). When the current density was 100, 200, 400, and 800 mA/g, the needle-like ZnO electrode showed average reversible capacities of 854, 635, 413, and 246 mAh/g, respectively.

**Figure 4.** (A) Cycling performance and (B) rate performance of the ZnO-10 and ZnO-60 electrodes.

#### 4. CONCLUSIONS

The deposition of ZnO nanoparticles on cotton fibers through ultrasonic irradiation was reported in this study. The presence of the hexagonal phase of the crystalline metal oxide on the cotton fibers was confirmed by XRD. When applied as anode materials for lithium-ion batteries, the ZnO-10 electrode showed a more favorable rate capability and cyclic performance than the ZnO-60 electrode.

The nanorod subunits were responsible for the enhanced electrochemical performance, since they can provide extra active sites on ZnO for reversible lithium storage and can facilitate the migration of lithium ions and electrons by connecting the adjacent ZnO as “bridges” and decreasing the electron-transfer resistance of the electrode.

#### ACKNOWLEDGEMENT

This study is funded by Science and Technology Research and Development Program of Shaanxi Province(2016GY-013).

#### References

1. Y.Q. Su, Y. Zhu, D. Yong, M. Chen, L. Su, A. Chen, Y. Wu, B. Pan and Z. Tang, *Journal of Physical Chemistry Letters*, 7 (2016) 1484.
2. G.X. Du, Q. Xue, H. Ding and Z. Li, *International Journal of Mineral Processing*, 141 (2015) 15.
3. T.O. Owolabi, M. Faiz, S.O. Olatunji and I.K. Popoola, *Materials & Design*, 101 (2016) 277.
4. E.A. Jolley, M. Lewis and B.M. Znosko, *Chemical Physics Letters*, 639 (2015) 157.
5. J. Jayabharathi, M. Sundharesan, A. Prabhakaran and C. Karunakaran, *Rsc Advances*, 5 (2015) 9518.
6. E.S. Kumar, F. Mohammadbeigi, L.A. Boatner and S.P. Watkins, *Journal of Luminescence*, 176 (2016) 47.
7. Y. Zhang, L. Ming, R. Wei and Z.G. Ye, *Appl. Surf. Sci.*, 340 (2015) 120.
8. Y.Y. Wang, C.X. Xu, M.M. Jiang, J.T. Li, J. Dai, J.F. Lu and P.L. Li, *Nanoscale*, 8 (2016) 16631.
9. L. Fu, A. Wang, G. Lai, C.-T. Lin, J. Yu, A. Yu, Z. Liu, K. Xie and W. Su, *Microchim. Acta.*, 185 (2018) 87.
10. X. Zhang, Y. Wang, F. Hou, H. Li, Y. Yang, X. Zhang, Y. Yang and Y. Wang, *Appl. Surf. Sci.*, 391 (2016) 476.
11. L. Dallali, S. Jaziri and J. Martínez-Pastor, *Solid State Communications*, s 209–210 (2015) 33.
12. A.H. Adl, P. Kar, S. Farsinezhad, H. Sharma and K. Shankar, *Rsc Advances*, 5 (2015) 87007.
13. J.B.L. Martins, E. Longo and C.A. Taft, *International Journal of Quantum Chemistry*, 70 (2015) 367.
14. X. Li, S. Cheng, S. Deng, X. Wei, J. Zhu and Q. Chen, *Scientific reports*, 7 (2017) 40911.
15. L. Fu, A. Wang, G. Lai, W. Su, F. Malherbe, J. Yu, C.-T. Lin and A. Yu, *Talanta*, 180 (2018) 248.
16. B. Ghosh, S.C. Ray, M. Pontsho, S. Sarma, D.K. Mishra, Y.F. Wang, W.F. Pong and A.M. Strydom, *Journal of Applied Physics*, 123 (2018) 161507.
17. Y. Zhao, C. Ying, Q. Huang, Y. Deng, D. Zhou, D. Wang, W. Lu and H.L. Cui, *Microelectronic Engineering*, 169 (2017) 43.
18. V. Khranovskyy, I. Shteplyuk, L. Vines and R. Yakimova, *Journal of Luminescence*, 181 (2017) 374.
19. X.H. Huang, X.H. Xia, Y.F. Yuan and F. Zhou, *Electrochimica Acta*, 56 (2011) 4960.
20. F. Belliard and J.T.S. Irvine, *Journal of Power Sources*, s 97–98 (2001) 219.
21. G. Yuan, G. Wang, H. Wang and J. Bai, *Ionics*, 21 (2015) 365.
22. G. Zhang, S. Hou, H. Zhang, W. Zeng, F. Yan, C.C. Li and H. Duan, *Adv. Mater.*, 27 (2015) 2400.
23. Y. Zhao, X. Li, L. Dong, B. Yan, H. Shan, D. Li and X. Sun, *International Journal of Hydrogen Energy*, 40 (2015) 14338.
24. P. Li, Y. Liu, J. Liu, Z. Li, G. Wu and M. Wu, *Chem. Eng. J.*, 271 (2015) 173.
25. B. Oschmann, M.N. Tahir, F. Mueller, D. Bresser, I. Lieberwirth, W. Tremel, S. Passerini and R. Zentel, *Macromolecular Rapid Communications*, 36 (2015) 1075.

26. S. Yamabi and H. Imai, *Journal of Materials Chemistry*, 12 (2002) 3773.
27. L. Vayssieres, *Adv. Mater.*, 15 (2003) 464.
28. P. Li, Y. Wei, H. Liu and X. Wang, *Chemical Communications*, (2004) 2856.
29. N.E. Blanchard, B. Hanselmann, J. Drost, M. Heuberger and D. Hegemann, *Plasma Processes & Polymers*, 12 (2015) 32.
30. R. Barakov, N. Shcherban, P. Yaremov, S. Gryn, V. Solomakha, I. Bezverkhyy, N. Kasian and V. Ilyin, *Journal of Materials Science*, 51 (2016) 4002.
31. A.A. Jahnke, L. Yu, N. Coombs, A.D. Scaccabarozzi, A.J. Tilley, P.M. Dicarmine, A. Amassian, N. Stingelin and D.S. Seferos, *Journal of Materials Chemistry C*, 3 (2015) 3767.
32. E. Ertas, İ. Demirtas and T. Ozturk, *Beilstein Journal of Organic Chemistry*, 11 (2015) 403.
33. L. Fu, A. Wang, F. Lyv, G. Lai, H. Zhang, J. Yu, C.-T. Lin, A. Yu and W. Su, *Bioelectrochemistry*, 121 (2018) 7.
34. W.Z. Wang, S. Meng, M. Tan, L.J. Jia, Y.X. Zhou, S. Wu, X.W. Huang, Y.J. Liang and H.L. Shi, *Applied Physics A*, 118 (2015) 1347.
35. S. Chouhan, R. Bhatt, A.K. Bajpai, J. Bajpai and R. Katore, *Fibers & Polymers*, 16 (2015) 1243.
36. K. Zhao, X.X. Song, C.S. Liang, J. Wang and S.A. Xu, *Iranian Polymer Journal*, 24 (2015) 425.
37. M. Ferbinteanu, F. Cimpoesu and S. Tanase, *Structure & Bonding*, 163 (2015) 185.
38. Y. Wu, J. Liu, C. Wu, Q. Zhuang, H. Chen, H. Zhang and X. Zhang, *Ionics*, 21 (2015) 635.
39. T. Pecchioli, M.K. Muthyala, R. Haag and M. Christmann, *Beilstein Journal of Organic Chemistry*, 11 (2015) 730.
40. R. Wang, J.H. Xin, X.M. Tao and W.A. Daoud, *Chemical Physics Letters*, 398 (2004) 250.
41. I. Perelshtein, G. Applerot, N. Perkash, E. Wehrschuetz-Sigl, A. Hasmann, G. Guebitz and A. Gedanken, *Surface and Coatings Technology*, 204 (2009) 54.
42. O. Garcia-Martinez, R. Rojas, E. Vila and J.M. De Vidales, *Solid State Ionics*, 63 (1993) 442.
43. M.Y. Ghotbi, *J. Alloy. Compd.*, 491 (2010) 420.
44. H. Wang, Q. Pan, Y. Cheng, J. Zhao and G. Yin, *Electrochimica Acta*, 54 (2009) 2851.
45. X. Huang, X. Xia, Y. Yuan and F. Zhou, *Electrochimica Acta*, 56 (2011) 4960.
46. Q. Xie, X. Zhang, X. Wu, H. Wu, X. Liu, G. Yue, Y. Yang and D.-L. Peng, *Electrochimica Acta*, 125 (2014) 659.
47. X. Wang, G. Wang, G. Zhai and H. Wang, *Journal of Materials Research*, 29 (2014) 1393.
48. X. Wang, J. Rong, Y. Song, X. Yu, Z. Zhan and J. Deng, *Physics Letters A*, 381 (2017) 2845.
49. W. Li, K. Shang, Y. Liu, Y. Zhu, R. Zeng, L. Zhao, Y. Wu, L. Li, Y. Chu and J. Liang, *Electrochimica Acta*, 174 (2015) 985.
50. Y. Zhong, Y. Ma, Q. Guo, J. Liu, Y. Wang, M. Yang and H. Xia, *Scientific reports*, 7 (2017) 40927.
51. J.-Y. Liao, D. Higgins, G. Lui, V. Chabot, X. Xiao and Z. Chen, *Nano letters*, 13 (2013) 5467.
52. N. Liu, J. Shen and D. Liu, *Electrochimica Acta*, 97 (2013) 271